Astron. Astrophys. 364, 799–815 (2000)

ASTRONOMY AND ASTROPHYSICS

Sensitivity of the GOLF signal to combined solar velocity and intensity variations

R.K. Ulrich[1], **R.A. García**[2], **J.-M. Robillot**[3], **S. Turck-Chièze**[2], **L. Bertello**[1], **J. Charra**[4], **H. Dzitko**[2], **A.H. Gabriel**[4], **and T. Roca Cortés**[5]

[1] Department of Physics and Astronomy, UCLA, Los Angeles, CA 90095-1562, USA
[2] Service d'Astrophysique, DSM/DAPNIA, CE Saclay, 91191 Gif-sur-Yvette, France
[3] Observatoire de l'Université Bordeaux I, B.P. 89, 33270 Floirac, France
[4] Institut d'Astrophysique Spatiale, CNRS/Université Paris XI, 91405 Orsay, France
[5] Instituto de Astrofísica de Canarias, 38205 La Laguna, Tenerife, Spain

Received 10 May 1999 / Accepted 26 July 2000

Abstract. The GOLF instrument provides a stable and continuous measurement of the intensity of spatially integrated sunlight in one wing of the sodium D lines. Because the detected radiation results from atomic scattering, the GOLF signal can be traced to an atomic reference wavelength. The planned operations were to involve a form of relative photometry through the use of measurements on both the blue and red wings of the solar D lines of neutral sodium. However, due to the occasional malfunction of the polarization subsystem a "one wing photometric mode" operational alternative has been selected in order to ensure achievement of a 100% duty cycle. In this case, the signal observed consists of two photometric measurements at only one wing of each line of the sodium doublet separated by $g \times 0.43$ picometers (pm). The sodium cell system in GOLF combines photons scattered at three different wavelengths: one at D_1 and two at D_2. This paper developes a formalism to describe this system in terms of the solar spectral line profiles. A method of converting the one wing data to an effective velocity scale is presented. The method is applied to the nearly continuous 804 day sequence received from the GOLF instrument prior to the loss of telecommunications with SOHO on 24-June-1998. The resulting time sequence is part of the GOLF archive and can be made available to investigators. This publication describes some properties of this time series.

Key words: Sun: atmosphere – Sun: oscillations

1. Introduction

1.1. General background

The GOLF instrument is a resonant scattering spectrophotometer which measures the intensity of solar radiation at selected positions within the sodium doublet lines. The integrated sunlight is scattered by sodium vapor in a temperature controlled cell which is inside a permanent magnet at a position where the magnetic field is nearly uniform. The scattered wavelengths are governed by the magnetic field strength and by a combination of polarizing elements. An electromagnet modulates the magnetic field permitting the selection of two closely spaced positions on the line wings. Two of the polarizing elements include mechanisms which can rotate these elements in steps of 90 degrees to select either the blue or red wing of the sodium doublet lines. Full descriptions of the instrument and its early performance are to be found in Gabriel et al. (1995, 1997), and a discussion of system stability is given in Robillot et al. (1998). Due to occasional malfunction of the rotating mechanisms, the polarizers were stopped on 11 April 1996 at positions which select the blue wings of the lines and have been left fixed subsequently. The usual operation of a resonance cell system provides intensity measurements for both the blue and red line wings and the velocity is found from the ratio of the intensity difference to the intensity sum. In the stopped or single-wing mode no observations are available from the red side of the lines so that we cannot calculate the above ratio which leads to a velocity measurement where absolute photometric effects cancel out. Data taken between January 19 and April 1, 1996 include observations of both wings and this data is very helpful in determining instrumental properties.

Subsequent to April 11, 1996 the instrument functions largely in a photometric mode where variations over various time scales are combinations of intensity and velocity fluctuations. The purpose of this work is to show how the photometric signal can be converted to an effective velocity with a well determined scale. Essential to the success of this method is knowledge of the modulation of the field strength by the electromagnet. This method deduces the solar line profile from a combination of the magnetic modulation and the orbital velocity variations. There are basically two steps in the analysis: first, the raw signal C is converted to a photometric signal P through the correction for known instrumental and geometric effects as will be described by García et al. (2000) and second, a solar profile corrected signal S is calculated from P by correcting for the deduced variation in the net solar profile intensity. Although

Send offprint requests to: R.K. Ulrich (ulrich@astro.ucla.edu)

Table 1. Sequence of data flow and data products

Varib.	Description	Reduction Steps
C	Photomultiplier Counts	Data stream reformatted into one fits file per day.
P	Photometric Rate	Corrections applied: 1. Deadtime 2. Stem temperature 3. Sun-spacecraft distance
S	Signal	The photometric rate is corrected for spectral line intensity which depends on sun-spacecraft velocity.
v	Velocity	The signal is corrected for long time-scale drifts (over 60 day periods) and multiplied by a velocity scale factor V_0.

no temporal filtering is required in the calculation of S substantial long time-scale trends remain. These can either be removed by introducing a temporal filter or through the application of a model for the trends. Such a model is presented below in Sect. 6 and time series which retain components with periods shorter than about 80 days are derived. The remaining detrended signal is then converted to a velocity variation through the multiplication of the residual signal by a derived sensitivity function V_0. These velocity time series have been placed in the GOLF/SOHO archive. The key steps and data products are summarized in Table 1.

The approach we use here allows us to study the power spectrum shape over a wide range of frequencies. From this spectrum which is presented it Sect. 7.1 we identify a break in the slope at 25 μHz. Below this frequency the power appears to come from solar activity whereas above the break the power spectral shape more resembles that due to convection. This distinction may be helpful in the formulation of strategies to find low frequency modes of oscillation. In addition, the derived solar profile permits a conversion between the intensity variation and an equivalent velocity shift using a known factor which depends on the sun-spacecraft line-of-sight velocity. Thus the rms variations in intensity which are a consequence of both the rms velocity amplitude and the time dependent line slope can have the latter factor removed and we are able to study the variation of the rms velocity itself in the 5-minute band as a function of orbital velocity. Because the orbital velocity causes the height of formation of the GOLF working point to shift through the solar atmosphere, we can determine the height dependence of oscillation amplitude.

1.2. Velocity versus intensity

The question of intensity versus velocity sensitivity can be discussed directly in terms of the data using a comparison with other instruments having known characteristics. An important technique in this regard is the study of phase relations between various signals. Pallé et al. (1999) and Renaud et al. (1999) have determined phase angles for modes in the five-minute band and concluded the GOLF signal is predominantly due to velocity. Gabriel et al. (1995) shows a comparison between a one-wing power spectrum derived from the ground-based comparison calibration and the two-wing power spectrum. Ulrich et al. (1998) compares power spectra based on the S method, an alternative method and the two-wing power spectrum. All three of these comparisons show that the one-wing power is greater than the two wing power for frequencies less than the 5-minute band. Since the intensity contribution is significantly reduced for the two wing method, this comparison suggests that the balance between intensity and velocity depends on whether the variations are caused by coherent oscillations or by the solar noise.

While the issue of the intensity versus velocity contribution is of concern, the primary objective of this paper is to explicitly describe a series of steps which can convert the raw GOLF signal into a quantity which has units of velocity and present some results based on this analysis. The first 6 months of the resulting data sets are now publically available on the web at: `http://www.medoc-ias.u-psud.fr/golf/`. The remainder will be released shortly. The method described here is unable to make a distinction between these two components and treats the conversion as if the signal variations are caused by velocity changes alone. Extensions of this treatments utilizing additional data may provide a distinction between the intensity and velocity components of the GOLF signal and will be discussed in future papers. However, it must be recognized that the GOLF signal reduced to the S quantity inherently contains a contribution from intensity which cannot be evaluated based on the GOLF data alone. This intensity is for a point relatively close to the core of a strong resonance line and differs considerably from the continuum intensity so that its role in the oscillations is difficult to estimate theoretically. However, correlation with magnetic activity indicies provides a method of estimating the effects of this component of non-velocity signal.

1.3. Interaction of the instrument and solar line radiation

Preliminary discussions of the reduction of the GOLF data have been given by García et al. (1998), Robillot et al. (1998), and Ulrich et al. (1998) while García et al. (2000) provide details of another method of velocity scaling the GOLF signal. The first of these papers describes the development of a model data stream composed of contributions from oscillations and supergranular convection. The second describes corrections to the raw intensity and presents some alternate formulations to treat the single wing data. The third gives a summary of two data reduction methods and compares the implied velocity output for these two methods. A related paper to follow by Ulrich et al. (2000) extends the method developed here to incorporate data from spatially resolved images from the MDI experiment on SOHO.

We consider the scattered light signal from the system to be governed by two tunable parameters: a) the wing selection polarizing elements, which we denote by subscripts b and r for

red and blue wings, and b) the modulation state of the electromagnet, which we denote by a superscript $+$ or $-$. For parts of the time sequence during the two-wing mode of operation two additional parameters: a second rotating polarizing element and a 180° redundancy in one retarding polarizer element, played a role in the data. For the two wing analysis we combine and average the separate data streams from these parameters.

The GOLF instrument system utilizes both D_1 and D_2 lines. Due to telluric absorption components near the working point on the red wing of D_2, no meaningful groundbased tests of the integrated system were possible and the evaluation of the properties of the instrument must be carried out using the operational data from space. The use of both members of the doublet complicates the interpretation of the GOLF signal due to fact that at any moment three separate wavelength bands are scattered into the detection chain. We designate as λ_1, $\lambda_{2\mathrm{a}}$ and $\lambda_{2\mathrm{b}}$ the longitudinal Zeeman components which are offset from the non-magnetic wavelengths $\lambda_{0,1} = 589.5924$ nm and $\lambda_{0,2\mathrm{a}} = \lambda_{0,2\mathrm{b}} = 588.9950$ nm (Reader & Corliss 1950) to wavelengths of

$$\begin{aligned} \lambda^{\pm}_{b,i} &= \lambda_{0,i} - g_i(\Delta\lambda_B \pm \delta\lambda_B) \\ \lambda^{\pm}_{r,i} &= \lambda_{0,i} + g_i(\Delta\lambda_B \pm \delta\lambda_B)\ . \end{aligned} \tag{1}$$

For a permanent magnetic field of strength B_0 and an electromagnet modulation of δB the wavelength increments are:

$$\Delta\lambda_B = A\,B_0 \quad , \quad \delta\lambda_B = A\delta B \tag{2}$$

with Zeeman factors of

$$(g_1, g_{2\mathrm{a}}, g_{2\mathrm{b}}) \;=\; (4/3, 5/3, 3/3) \tag{3}$$

and following Boumier (1991) we have used the notation $i = 1, 2a, 2b$. The magnetic conversion factor A is 1.62×10^{-6} for magnetic fields in gauss and wavelengths in nm and we have neglected a small difference in the value of A for the D_1 and D_2 lines.

The design of the GOLF magnet provides a field at the sodium cell which is sufficiently uniform that $\Delta\lambda_B$ can be taken as a constant for all scattered photons. The scattering process is broadened by the presence of hyperfine states in the upper and lower atomic states and by the thermal motions of the sodium atoms in the cell. These later processes dominate over the magnetic field non-uniformities and each scattering component is roughly described by a gaussian with a width parameter σ of about 1.3 pm while the $\Delta\lambda_B$ values range between 8.0 and 13.8 pm. Thus the sampled portions of the solar spectral lines are well separated from each other. Through the use of the modulated electromagnet the magnetic field at the cell has two values: $B_0 + \delta B$ and $B_0 - \delta B$. The values of B_0 and δB are inferred by Gabriel et al. (1995) from prelaunched subsystem measurements of the wavelengths of the scattering components from the actual flight system. In addition, the value of δB is determined below from an analysis of the flight data.

Some care with notation is required in describing the GOLF system because of the variety of varying parameters: the multiple scattering wavelengths, the two distinct spectral lines, the magnetic modulation and the red or blue wing selection. In addition, we need to refer to actual intensities for a particular configuration and to spectral line profiles which are functions of a wavelength difference. The sub and superscript notation was given above. In order to make a clear distinction between a realized intensity and a line profile function, we use math italic for the intensities as I^+_b refers to the intensity in the blue wing with the positive state of the electromagnet. This intensity will generally depend on the sun-spacecraft velocity but we do not explicitly designate this dependence. For a line profile function we use bold face and explicitly give the function on which it depends: $\mathbf{I}_{\lambda,j}\{w,t\}$ is such a profile function for spectral line j depending on w which has dimensions of wavelength. The indicated time dependence comes primarily from the transit of active regions across the solar disk and is neglected for most of this discussion.

The GOLF system avoids the need for a filter to separate the two sodium D line components by measuring both lines. The absence of such a filter improves system stability but comes at the price of introducing some uncertainty in knowledge of the balance between the three scattering components. Boumier (1991, see also Boumier & Damé 1993) has modelled the transfer of radiation within the sodium cell and successfully simulated the wavelength dependence of the scattered light as a function of cell gas temperature. Subsequent subsystem tests described by Boumier et al. (1994) have validated his simulation. Fig. 1 shows two measured scattering profiles from these prelaunched tests, σ_λ, at gas temperatures of about 155° and 163° C. The scale shown for σ_λ is based on the comparison of the photomultiplier outputs for the straight-through beam to the scattered beam and is uncertain on an absolute basis. However, the relative intensities between the different scattering components has an uncertainty of 5%. For comparison the observed integrated sunlight profiles measured by Delbouille et al. (1973) are shown in Fig. 1 shifted in such a way that they both coincide with the scattering functions. The solar line is shifted from this position by a combination of orbital motion, Einstein shift and a third effect known as the convective correlation shift which is caused by the enhanced brightness of the hotter, rising convective cells relative to the cooler, sinking cells. The convective correlation shift depends on altitude in the solar atmosphere and can alter the spectral line shapes. The details of this process are not well enough understood to permit a reliable calculation of the shifts.

At low cell gas temperature all scattering components increase in strength in proportion to the gas density and maintain a constant relative ratio. However, at cell gas temperatures above about 140° C, the $D_{2\mathrm{b}}$ component which has the largest scattering cross-section progressively saturates and makes a reduced relative contribution to the detected signal. This effect is evident by comparing the scattering profile at $D_{2\mathrm{b}}$ in Fig. 1. Because the solar line slope differs at each of the scattering wavelengths, the balance between the three scattering components influences the conversion factor between intensity variations and velocity. Consequently, we need to know the cell gas temperature in order to properly analyze the GOLF signal. A platinum temperature probe near the sodium cell stem provides an important indica-

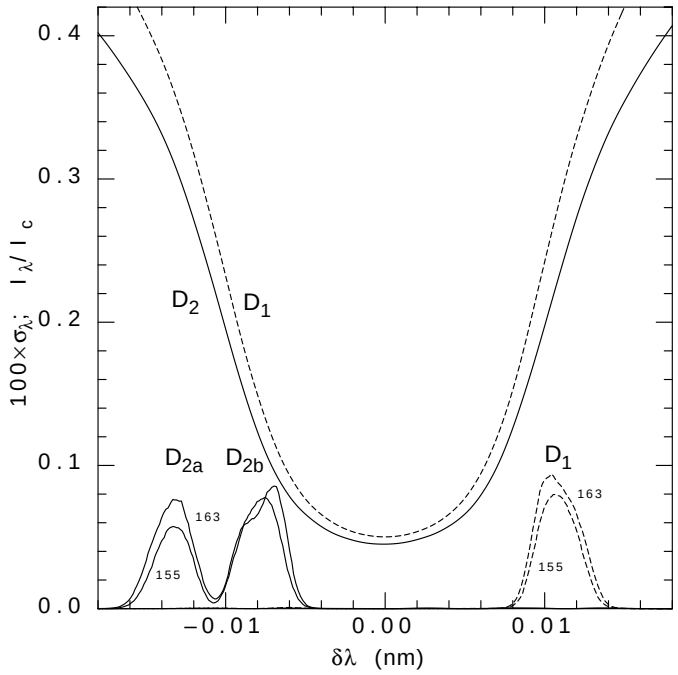

Fig. 1. Comparison of the sodium cell scattering functions, σ_λ, to the observed integrated-sunlight line profiles of the two sodium D lines. The scattering functions for D_2 are shown as solid on the blue wing while the scattering function for D_1 is shown on the red wing. Both the observed solar line profiles and the scattering functions have been shifted so as to have their central wavelengths coincide. The scattering functions in fact are both selected to be on the blue or red wings by the alignment of the rotational orientation of the polarizer optics. They are shown here on opposite wings for clarity.

tion of the critical temperature but there is a poorly known offset between this measurement and the actual gas temperature.

Two instrumental quantities necessary for a full interpretation of the GOLF data are the on-orbit magnetic field modulation amplitude and the temperature of the gas in the sodium cell. Preflight subsystem tests were carried out to obtain these quantities. The early two wing observations between Jan. 19 and Apr. 1, 1996 are used here to determine the magnetic modulation based on the known variation in the sun-spacecraft velocity. The same observation period permits an estimation of the cell gas temperature by comparison of the observed intensity ratios as a function of orbital velocity to the average of integrated sunlight line profiles weighted by factors dependent on the cell gas temperature.

In this paper we utilize the magnetic modulation to deduce the average solar line profile as a function of orbital velocity and thus reduce the observed signal to photometric quantity independent of the orbital velocity induced variations. This method is directly dependent on all instrumental drifts and decays in sensitivity. Although it is necessary to estimate the long term trends in the instrument, because no other smoothing is done during the reduction, it is possible to preserve phenomena on longer time scales. The range of frequencies preserved in the analysis is limited primarily by the detrending process which does not include a formal temporal filter but instead utilizes a somewhat complex functional fitting procedure. In some cases it is desireable to impose an additional hard frequency cutoff with a high-pass filter. The detrending strongly reduces the spectral power on time scales longer than 60 days but leaves it largely unchanged for time scales shorter than 45 days. A hard cutoff of 60 days is generally used to assure that the poorly fit spectral components with time scales longer than this do not leak into the higher frequency spectra. Furthermore, since each phase of the magnetic modulation is treated independently, the analysis yields four independent data sets – two for each photometer channel.

The remainder of this paper consists of five parts: Sect. 3 uses data from the two-wing period of operation to determine the amplitude of magnetic modulation; Sect. 5 describes our method of converting the photomultiplier output into a velocity result; next, a Sect. 6 applies the method to the GOLF data and presents time series analysis based on the detrended velocity data set; and finally a Sect. 7 presents results for the deduced power spectra extending from $0.2\ \mu$Hz to $6000\ \mu$Hz and the time dependence of the rms velocity in the 5-minute band.

2. Scattering strengths

The magnetic field measurements carried out during the subsystem analysis of the GOLF instrument described by Gabriel et al. (1995) yielded both the magnetic field values and detailed profiles of the scattered light intensity as a function of wavelength. We describe in this section how the scattering profiles interact with the line profiles and provide a formalism for describing the combined output from the three scattering components.

Utilization of the full set of photomultipliers in place during the subsystem tests permited the determination of the scattering profile σ_λ in each of the Na D components. Of greatest importance to the deduction of the influence of the line profiles on the GOLF signal is the balance between the three scattering components. We define this balance by

$$\phi_i \;=\; A \int_{\lambda_1}^{\lambda_2} \sigma_\lambda \, d\lambda \tag{4}$$

where A is a normalization factor chosen so that $\sum_i \phi_i = 1$, and λ_1 and λ_2 are chosen to isolate as well as possible the separate scattering components. For D_1 using the red wing laser scans $\lambda_1(D_1) = 589.6003$nm and $\lambda_2(D_1) = 589.6103$nm while for D_2 using blue wing data $\lambda_1(D_{2a}) = 588.9783$nm, $\lambda_2(D_{2a}) = \lambda_1(D_{2b}) = 588.9845$nm and $\lambda_2(D_{2b}) = 588.9923$nm. The dependence of ϕ_i on cell gas temperature T_g is given in Table 2. These temperatures have been determined by comparison to the model calculations by Boumier et al. (1994). The platinum probe temperatures T_p are also given in Table 2. The temperatures used in evaluating the observed signal are based on T_p.

3. Determination of the magnetic modulation from two-wing observations

Although the data between January 19, 1996 and April 1, 1996 are perturbed by a variety of commissioning activities, it repre-

Table 2. Scattering strengths

$T_{\rm g}$ (C)	$T_{\rm p}$ (C)	$\phi_{\rm D_1}$	$\phi_{\rm D_{2a}}$	$\phi_{\rm D_{2b}}$
130	139	0.355	0.232	0.413
138	149	0.353	0.235	0.412
146	159	0.374	0.243	0.383
155	170	0.381	0.254	0.364
163	180	0.385	0.284	0.331
174	195	0.386	0.314	0.300

sents the only period during which both the blue and red wings of the Na D lines were observed from space with the GOLF system which includes the magnetic modulation. The classic resonance scattering helioseismometer yields an observable designated as R:

$$R \;=\; \frac{I_b - I_r}{I_b + I_r}\;. \tag{5}$$

The use of the modulated electromagnet permits a monitoring of the net solar line profile as averaged by the instrument. The amplitude of magnetic modulation can be found in addition through the use of the orbital changes in the sun-spacecraft velocity. The magnetic modulation combined with the wing selection by the rotating polarizers provides four measurable quantities: $(I_b^+, I_b^-, I_r^+, I_r^-)$. These can be combined to yield a number of different expressions for R like that of Eq. (5). First, if we take $I_b = (I_b^+ + I_b^-)/2$ and $I_r = (I_r^+ + I_r^-)/2$, we recover Eq. (5) exactly. Second following Boumier (1991), García (1996) and Boumier et al. (1991) we can define red and blue analogues of Eq. (5) as follows:[1]

$$R_b \;=\; \frac{I_b^+ - I_r^-}{I_b^+ + I_r^-} \tag{6}$$

$$R_r \;=\; \frac{I_b^- - I_r^+}{I_b^- + I_r^+} \tag{7}$$

If the scattering process included only one term instead of three, the difference between R_b and R_r would be the same as would result from a velocity shift equivalent to that implied by the separation between the wavelengths of the two states of magnetic modulation. The asymmetrically placed set of three scattering wavelengths causes the centroid of the combination to be dependent on the scattering gas temperature. We can estimate the effective value of the wavelength separation by smoothing each R function in time and then considering each to be a function of the orbital velocity plus an offset. If we represent these smoothed functions of velocity v by the notation: $\langle R_b\rangle(v)$ and $\langle R_r\rangle(v)$ then we should have $\langle R_b\rangle(v_{\rm orbital} + \delta v_R) = \langle R_r\rangle(v_{\rm orbital} - \delta v_R)$ for some value of δv_R. This suggests the strategy of plotting $\langle R_b\rangle$ versus $v_{\rm orbital} + \delta v_R$ and $\langle R_r\rangle$ versus $v_{\rm orbital} - \delta v_R$ so that if δv_R is properly chosen the two curves should coincide. Fig. 2 shows this comparison with $\delta v_R = 83.3 \pm 1\,{\rm m\,s^{-1}}$. This figure shows the full range of R values returned over this span of orbital velocity.

[1] We modify the notation of Boumier (1991) to use the quantities R_b and R_r in place of O^+ and O^- respectively because we later use the subscript R to denote quantities derived from differences between R_b and R_r where a subscript O could be confused with a subscript 0 and to emphasize the fact that all of the R quantities are formed from a similar combination of intensities.

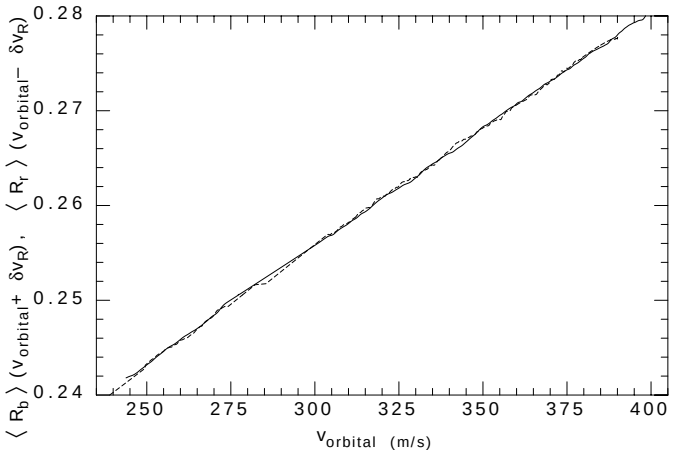

Fig. 2. Comparison of $\langle R_b\rangle$ and $\langle R_r\rangle$ as functions of orbital velocity $\pm\delta v_R = 83.3\,{\rm m\,s^{-1}}$. The curve for R_r is shown as dashed.

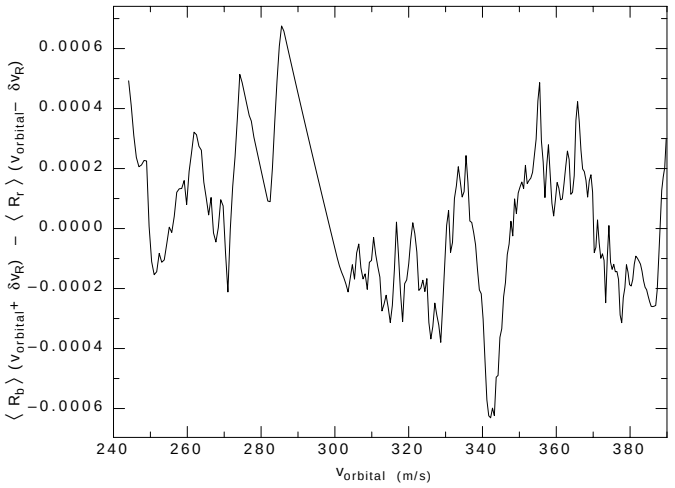

Fig. 3. The difference between $\langle R_b\rangle(v_{\rm orbital} + \delta v_R)$ and $\langle R_r\rangle(v_{\rm orbital} - \delta v_R)$ as functions of orbital velocity.

The value of δv_R which produces the most exact agreement between the R_b and R_r is uncertain due to irregularities in the longer term trends of the two functions. The magnitude of this uncertainty can be estimated by examining $\Delta\langle R\rangle = \langle R\rangle_b(v_{\rm orbital} + \delta v_R) - \langle R\rangle_r(v_{\rm orbital} - \delta v_R)$ as a function of $v_{\rm orbital}$ with δv_R as a parameter. This comparison is shown in Fig. 3. The value of δv_R determines the average value of $\Delta\langle R\rangle$ so that if δv_R is too small, $\Delta\langle R\rangle$ is positive and if δv_R is too large, $\Delta\langle R\rangle$ is negative. The correct δv_R leaves the average of $\Delta\langle R\rangle$ near zero. A figure of the merit for any choice of δv_R is $(\Delta\langle R\rangle)_{\rm rms}$, the rms variation in $\Delta\langle R\rangle$ considered as a function of $v_{\rm orbital}$. The best value of δv_R is that which minimizes $(\Delta\langle R\rangle)_{\rm rms}$. Due to the irregularities in the $\Delta\langle R\rangle$ function as shown in Fig. 3 this minimum is not precisely defined. The be-

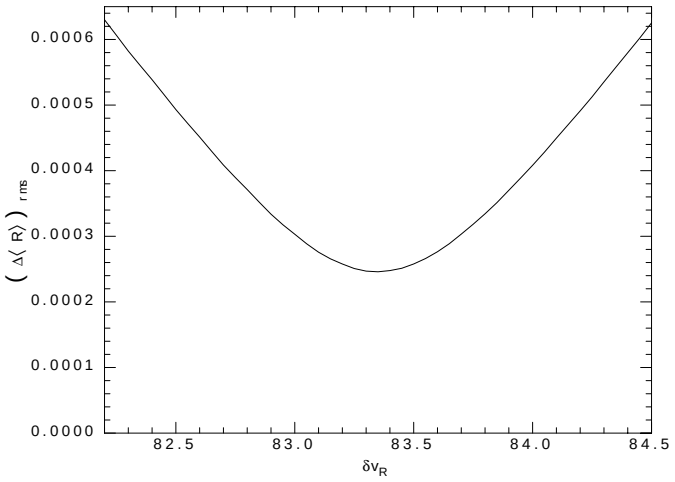

Fig. 4. The behavior of $(\Delta \langle R \rangle)_{\rm rms}$ as a function of δv_R.

havior of $(\Delta \langle R \rangle)_{rms}$ versus δv_R is shown in Fig. 4. The breadth of the minimum in Fig. 4 provides an estimate for the uncertainty of δv_R which is about $0.5\,{\rm m\,s^{-1}}$. Although this value is well determined and is based on signals which have been corrected for the known effects such as dead-time and resonance cell stem temperature variations, the observations were made during a period of the experiment when a variety of other parameters were undergoing adjustment. Therefore, there could be systematic effects which cause the above formal error to be an underestimate of the actual uncertainty in the δv_R parameter.

In order to convert δv_R into an effective magnetic field modulation amplitude we use the derivative of Eq. (5) to obtain a relationship between the line intensity slopes and δv_R:

$$\begin{aligned} \delta v_R &= \frac{dv}{dR}\,\delta R \\ &= \frac{1}{2}\frac{(I_b + I_r)^2}{I_r(dI_b/dv) - I_b(dI_r/dv)}\,\delta R\,. \end{aligned} \tag{8}$$

Next we need to relate the amplitude of magnetic modulation δB to δv_R and this requires consideration of the interaction between the solar line profile and the sodium scattering. Each scattering component has a wavelength λ_i according to Eq. (1). The sun-spacecraft velocity determines $\lambda_{\odot,i} = \lambda_{0,i}(1 + v/c)$ where v is the sum of orbital velocity, the Einstein shift velocity $v_E = GM_\odot/cR_\odot = 636\,{\rm m\,s^{-1}}$, convective correlation shifts v_c, and the velocity signal we wish to measure δv. The convective correlation shift is poorly determined theoretically and depends on the definition of the position of the solar line. Each solar line profile j can be considered as a function $\mathbf{I}_{\lambda,j}\{w\}$ where w is an input parameter having dimensions of wavelength as indicated by the subscript λ and the bracket notation indicates a functional relationship. In our case w is the wavelength difference between the scattering component and a centroid of the solar line. Each solar line profile $\mathbf{I}_{\lambda,j}\{\lambda - \lambda_\odot\}$ can be taken as a constant when averaged over long time periods. These represent the D_1 and D_2 integrated sunlight profiles. The observed intensities are then:

$$I_b^{\pm} = \sum_i \phi_i \mathbf{I}_{\lambda,j}\{\lambda_{b,i}^{\pm} - \lambda_\odot\} \tag{9}$$

$$I_r^{\pm} = \sum_i \phi_i \mathbf{I}_{\lambda,j}\{\lambda_{r,i}^{\pm} - \lambda_\odot\} \tag{10}$$

which yield:

$$I_b^{\pm} = \sum_i \phi_i \mathbf{I}_{\lambda,j}\{-g_i(\Delta\lambda_B \pm \delta\lambda_B) - \lambda_0 v/c\} \tag{11}$$

$$I_r^{\pm} = \sum_i \phi_i \mathbf{I}_{\lambda,j}\{+g_i(\Delta\lambda_B \pm \delta\lambda_B) - \lambda_0 v/c\}\,. \tag{12}$$

Eqs. (11) and (12) require knowledge of the line profiles over some range in v near each of the working points. For the full velocity range of the orbital motion of SOHO, the line profiles are significantly non-linear. For the purpose of the determination of the magnetic modulation, we may consider a restricted range as illustrated in Fig. 2 of $\pm 50\,{\rm m\,s^{-1}}$ in which case the profile is nearly linear. We may then define a reference velocity $v_{\rm ref}$ and consider $\delta v = v - v_{\rm ref}$ to be small along with the magnetic modulation velocity $\delta v_B = c\delta\lambda_B/\lambda_0 = (cA/\lambda_0)\delta B$. We may also consider the line profile to be a function of velocity instead of wavelength: $\mathbf{I}_{v,j}\{-(c/\lambda_0)x\} = \mathbf{I}_{\lambda,j}\{x\}$. After adopting the following compact notation for the derivative with respect to velocity:

$$\mathbf{I}'_{v,j} = \frac{d\mathbf{I}_{v,j}}{dv} = -\frac{\lambda_0}{c}\frac{d\mathbf{I}_{\lambda,j}}{d\lambda} \tag{13}$$

and defining:

$$I_{b,i} = \mathbf{I}_{v,j}\{-g_i\Delta v_B - v_{\rm ref}\} \tag{14}$$

$$I_{r,i} = \mathbf{I}_{v,j}\{+g_i\Delta v_B - v_{\rm ref}\} \tag{15}$$

$$I'_{b,i} = \mathbf{I}'_{v,j}\{-g_i\Delta v_B - v_{\rm ref}\} \tag{16}$$

$$I'_{r,i} = \mathbf{I}'_{v,j}\{+g_i\Delta v_B - v_{\rm ref}\} \tag{17}$$

and using a linear expansion about the reference velocity we obtain:

$$I_b^{\pm} = \sum_i \phi_i \left[I_{b,i} + I'_{b,i}(\pm g_i\delta v_B + \delta v)\right] \tag{18}$$

$$I_r^{\pm} = \sum_i \phi_i \left[I_{r,i} + I'_{r,i}(\mp g_i\delta v_B + \delta v)\right]\,. \tag{19}$$

Two properties of these definitions are worth emphasizing: first, even though we have used a velocity scale for the argument of the line profile function, we have reversed the sign in order to account for the fact that the velocity appears with a negative sign in Eqs. (14 - 17); and second, the slopes $I'_{b,i}$ are positive while the slopes $I'_{r,i}$ are negative.

We can now express the intensity change due to the magnetic modulation as

$$I_b^{\pm} = I_b \pm \delta I_b \qquad I_r^{\pm} = I_r \pm \delta I_r \tag{20}$$

with:

$$\delta I_b = \sum_i \phi_i |I'_{b,i}| g_i\,\delta v_B \qquad \delta I_r = \sum_i \phi_i |I'_{r,i}| g_i\,\delta v_B\,. \tag{21}$$

Utilizing the fact that $\delta I/I << 1$ we can write R_b as

$$R_b = \left(R + \frac{\delta I_b + \delta I_r}{I_b + I_r}\right)\left(1 + \frac{-\delta I_b + \delta I_r}{I_b + I_r}\right) \tag{22}$$

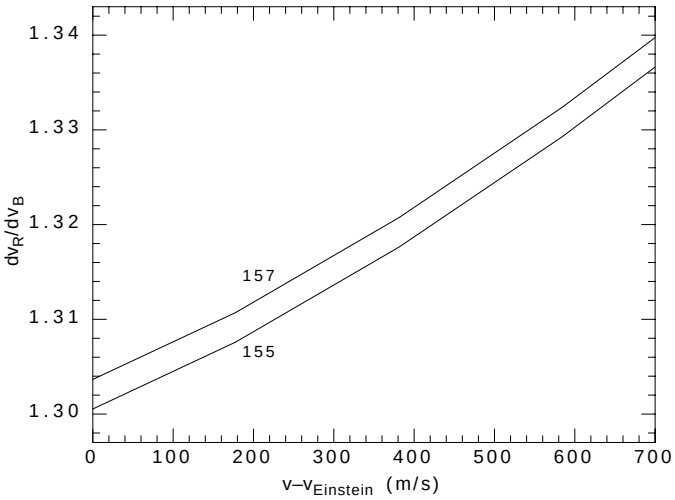

Fig. 5. The function dv_R/dv_B as a function of $v - v_{\rm Einstein}$. The derivative is dimensionless while the velocity differs from the orbital velocity by the convective velocity offset. The cell gas temperature is shown for each of the two lines. The values chosen bracket the range observed during the first year of operation. For the purpose of finding the magnetic modulation, we need the gas temperature during the two-wing period which ranged between 154.9° C and 155.1° C.

giving $\delta R = R_b - R$ which can be inserted into Eq. (8) to obtain:

$$\delta v_R = \frac{\sum_i \phi_i g_i \left(I_r |I'_{b,i}| + I_b |I'_{r,i}| \right)}{\sum_i \phi_i \left(I_r |I'_{b,i}| + I_b |I'_{r,i}| \right)} \delta v_B \equiv \frac{dv_R}{dv_B} \delta v_B. \quad (23)$$

Due to the temperature dependence of the scattering strengths ϕ_i, the value of dv_R/dv_B also depends on the temperature as well as the offset velocity. The total range in temperature as indicated by the platinum probe is from 169.9° C to 171.6° C during the entire first year of operation. During the two wing period which is of interest the range was restricted to 169.9° C to 170.2° C. This corresponds to a gas temperature between approximately 154.9° and 155.1° C where there is an uncertain offset to the true gas temperature. The dv_R/dv_B functions as derived from the Delbouille et al. (1973) integrated sunlight profiles are shown in Fig. 5. Since the offset velocity at the central time of the sequence was $315\,\mathrm{m\,s^{-1}}$, we can derive $dv_R/dv_B = 1.314 \pm 0.003$. From this result we may derive:

$$\delta v_B = 63.3 \pm 1\ \mathrm{m\,s^{-1}}\ . \quad (24)$$

The derived δv_B corresponds to a magnetic modulation of 76.9 ± 1 gauss. Eq. (24) provides a precise determination of the magnetic modulation amplitude and is adopted for the remainder of this paper.

4. Corrections to the photomultiplier outputs

The reduction sequence starts with the removal of instrumental effects along with the compensation for the inverse square effect of the variable distance. We refer to the output of this step as the photometric rate P. These steps will be described in García et al. (2000).

5. Conversion of the raw signal to a velocity scale

5.1. General considerations

In this section we describe an analysis of the GOLF signal based on the direct photometric signals. In this approach it must be recognized that we are using the signal in an absolute photometric mode – one of the most difficult tasks in observational astronomy. Other approaches such as that described by Robillot et al. (1998) utilize a ratio of signals so that most of the effects only enter in second order (note that all corrections are applied in that approach even though the deduced velocity is less dependent on the corrections than is the case with this method). For the direct photometric method, any instrumental drift will find its way into the signal and can masquerade as a solar velocity. The only reason we can attempt this approach is the great stability of the observing platform and instrument. We are also aided by the separation in frequency between most drifts which occur over periods longer than one day and the solar oscillation modes of interest which have periods in the 0.05 to 3.0 hour range. However, there are also some gain fluctuations mostly from PM1 which produce abrupt jumps in this photomultiplier's counting rate and if uncorrected would add noise to the data in a frequency band overlapping that of interest. These events are mostly discrete and small in number and have been removed by applying a compensating discontinuity which is adjusted to assure smoothness across the jump.

In the face of these obstacles it may seen undesireable to use a direct photometric approach for the conversion of the GOLF signal into a quantity having dimensions of velocity. Our motivation is as follows: a prime objective of the GOLF project is to identify for the first time coherent solar oscillations in the period range 0.5 to 3.0 hours. Our ability to make this identification is improved if we understand the sources of non-coherent velocities and develop methods of modeling them from other data. The photometric signal is an integral of the intensity over the visible solar disk so that the full disk intensity can be considered to be a linear combination of the intensities produced by an array of pixel-sized sub-elements. If we can deduce the pixel by pixel signal due to non-coherent processes through the use of data from the MDI instrument on SOHO combined with ground-based observatory data, we can form the linear combination of these effects with those due to velocities and possibly correct for the non-coherent processes. The linear dependence present in treating the signal as photometric eases the task of isolating these effects. At shorter oscillation periods we can compare GOLF to other oscillation observations while at longer periods we can identify and possibly study the effect of solar active regions and supergranulation on the GOLF measurements. In this way we may be able to work our way into the $g-$mode frequency range from above and below.

In the above context conversion to a velocity scale takes the form of a function of the observed signal as follows:

$$v = V_0(t)\left(\frac{S(t) - S_0(t)}{S_0(t)}\right) \tag{25}$$

where $S_0(t)$ is an intensity-like signal that is a very slowly changing function of time including all identifiable properties of the instrument and orbit as well as the solar line profiles. The observed intensity $S(t)$ is a similarly corrected quantity derived from the moment by moment observation of the solar output. The sensitivity function V_0 is well-known as a critical parameter for resonance scattering instruments and is related to S_0 by:

$$V_0 = S_0\left(\frac{dS_0}{dv}\right)^{-1} \approx I_b\left(\frac{dI_b}{dv}\right)^{-1} . \tag{26}$$

It is important to note that even a perfect photometer system would not function as indicated in Eq. (25) because of the very large variations caused by the sun-spacecraft velocity variations and the consequent migration of the GOLF scattered wavelength relative to the solar spectral line. This subsection describes a method for calculating this effect.

The transformation from the observed count rate which we designate as $C(t)$ to an intensity-like variable allowing a velocity calculation of the form given in Eq. (25) requires a series of steps having varying degrees of reliability. The reduction sequence starts with the removal of instrumental effects along with the compensation for the inverse square effect of the variable distance. These steps will be described in García et al. (2000). These corrections for deadtime, stem temperature, the inverse square law and PM aging are all included here in deriving P, the photometric counting rate. Note, however, that the *known* correction for PM aging does not account for the full effects instrumental aging and this process is modelled in a more flexible fashion below. Correction for the effect of the variable distance and stem temperature can either increase or decrease the signal. The aging effects monotonically decrease the signal following a function which is probably roughly an exponential decay with and unknown decay rate. The first step in the reduction is then to correct the raw count rate $C(t)$ to a photometer rate $P(t)$ through the application of the deadtime correction, the inverse square distance correction and the stem temperature correction.

5.2. Use of the magnetic modulation

The corrections above are due to instrumental effects and the geometric inverse square effect of the variable distance. In addition there is the effect of the variable sun-spacecraft velocity on the solar line intensity at the working point of the GOLF instrument. This effect produces the instrument's sensitivity to velocity and is essential to the instrument operation. However, the large amplitude of velocity variation through the orbital path maps out a significant portion of the solar line profile and complicates the interpretation of the absolute photometry through the non-linearity of the functional relationship between velocity and intensity. Fortunately due to the magnetic modulation we have a method available to determine to a good approximation

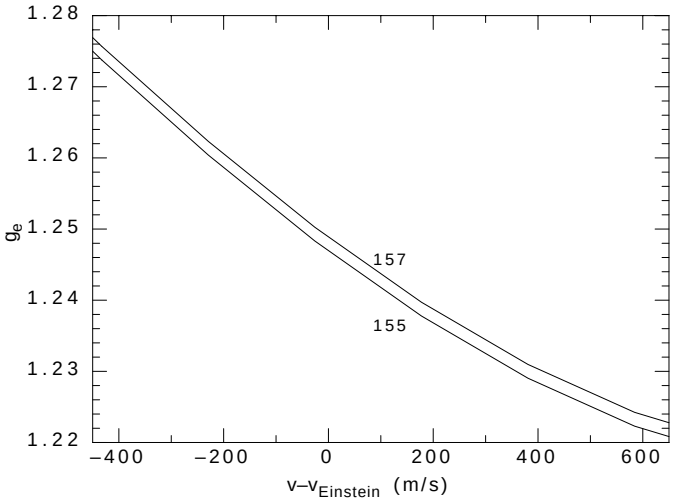

Fig. 6. The function g_e as a function of $v_{\rm orb} = v - v_{\rm Einstein}$. The derivative is dimensionless while the velocity differs from the orbital velocity by the convective velocity offset. The cell gas temperature is shown for each of the two lines. The values chosen bracket the range spanned during operations.

the combined solar line profile as seen by GOLF. At positive and negative magnetic modulation states we obtain photometric rates P^+ and P^- which correspond to a velocity difference δv which is an effective velocity offset between the two states of magnetic modulation. In essence we can use the difference in signal $\delta P(t) = P^+(t) - P^-(t)$ to estimate the derivative $P' = dP/dv$. By tracking the data over a large range in v, we can numerically integrate $P'dv$ to get $P(v)$ itself. This task suffers from the same difficulty of any absolute photometry in that $P(t)$ includes all the system gain uncertainties. We can overcome this problem by utilizing the ratio P^+/P^- as a function of time and orbital velocity since all gain uncertainties cancel in the ratio. Consequently, we have

$$\frac{P^+}{P^-} \;=\; \frac{I_b(v_{\rm orb} + \delta v)}{I_b(v_{\rm orb})} \equiv \frac{I_b^+}{I_b^-} \tag{27}$$

where we can express the ratio of the two intensities in terms of an effective velocity offset given by:

$$\delta v \;=\; \frac{\sum_i \phi_i g_i I_i'}{\sum_i \phi_i I_i'} 2\delta v_B \equiv g_e(2\delta v_B) \tag{28}$$

which defines g_e as an effective g value. This function is shown in Fig. 6 and is fit by:

$$g_e \;=\; 1.2491 - 5.084 \times 10^{-5} v_{\rm orb} \equiv \frac{\gamma_0 + \gamma_1 v_{\rm orb}}{2\delta v_B} \tag{29}$$

with $v_{\rm orb}$ in $\mathrm{m\,s^{-1}}$. We thus find that the orbital velocity plus the offset velocity is:

$$v_{\rm orb} + \delta v \;=\; (1+\gamma_1)v_{\rm orb} + \gamma_0 = (1+\gamma_1)(v_{\rm orb} + v_e) \tag{30}$$

where $v_e = \gamma_0/(1+\gamma_1)$. Using the value of δv_B from Eq. 24, we have $\gamma_0 = 158.1\,\mathrm{m\,s^{-1}}$, $\gamma_1 = -6.436 \times 10^{-3}$, and $v_e = 159.1\,\mathrm{m\,s^{-1}}$.

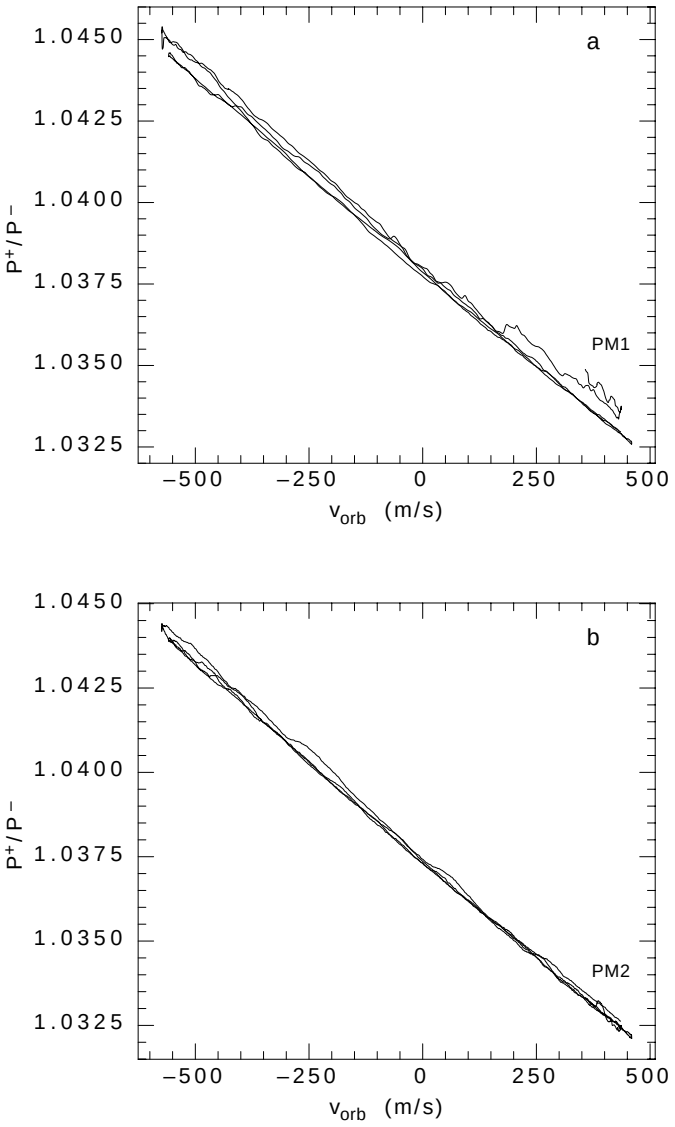

Fig. 7a and b. The magnetic modulation ratio P^+/P^- for the two photomultipliers as a function of the orbital velocity $v_{\rm orb}$. The upper subfigure **a** shows the function for PM1 and the lower subfigure **b** shows the function for PM2.

As long as the photomultipliers respond linearly to solar radiation the ratio P^+/P^- should be a function of orbital velocity alone. Thus we can express this ratio as a power series expansion:

$$\frac{P^+}{P^-} \;=\; 1 + \sum_{k=0}^{K} A_k \, v_{\rm orb}^k \approx \frac{I_b^+}{I_b^-} \tag{31}$$

where $K = 2$ for our present data. We could also consider K to be larger than 2 with the coefficients $A_k = 0$ for $k > 2$. In practice the data can be adequately fit with just A_0, A_1, and A_2 and inclusion of higher terms would raise the risk of fitting spurious features. Figs. 7a and 7b show the relationship between $v_{\rm orb}$ and P^+/P^- for PM1 and PM2. These figures include all data between April 11, 1996 and Feb. 16, 1998 except for the 5 day interval in Nov, 1996 when the GOLF system experienced a brief cooldown where the missing data has been replaced with an interpolated fill. For PM2 the ratio remains a unique function of $v_{\rm orb}$ whereas for PM1 the most recent data near $+350\,{\rm m\,s^{-1}}$ deviates from the previous pattern. Generally the data from PM2 appears more reliable than that for PM1.

Table 3. Fitting coefficients for the magnetic modulation ratio

	Wing	A_0	A_1 $({\rm m\,s^{-1}})^{-1}$	A_2 $({\rm m\,s^{-1}})^{-2}$
PM1	Blue	0.037885	-1.163×10^{-5}	0.73×10^{-9}
PM2	Blue	0.037341	-1.157×10^{-5}	0.69×10^{-9}
PM1	Red	0.052112	1.130×10^{-5}	-1.20×10^{-9}
PM2	Red	0.052108	1.085×10^{-5}	-0.55×10^{-9}

Although not needed for the primary data set beginning April 11, 1996, the magnetic modulation on the red wings of the lines is also of interest as a diagnostic of instrument performance and as a tool for verification of the analysis method. Table 3 gives both the fitting coefficients for the correlations shown in Figs. 7a and 7b and for similar correlations obtained for the red wing data between Jan. 20, 1996 and April 1, 1996. The blue wing coefficients apply to the full data set while those for the red wing are available only for these early operations. The red wing data in particular have been contaminated by a variety of commissioning activities and are less reliable for this reason as well as having reduced reliability due to the smaller range in orbital velocity spanned by the sequence.

5.3. Correction for the working point wavelength variation due to sun-spacecraft velocity changes

As the velocity of the spacecraft relative to the sun varies through the orbit, the intensity of the solar lines should change due to the shift of the central wavelength of the solar line relative to the fixed wavelengths of the scattering points. We wish to correct the output of the GOLF instrument for this effect by deducing the effective shape of the solar line from the magnetically modulated position of the scattering points and the drift in relative velocity itself. The line profiles have been defined in Eqs. 9, 10, 18 and 19. Whereas most of the discussion has been carried out in terms of ratios of outputs in order to eliminate the need to use absolute photometry, the line profile functions required in above equations are not written in the form of a ratio. They can be converted to a ratio by the adoption of a reference intensity defined to be I_0. A convenient choice of I_0 is that where the sun-spacecraft relative velocity is zero using the low field state of magnetic modulation.

To illustrate the method of obtaining the line intensity from the observed ratio of intensities in the two magnetic modulation states, we retain only A_1 and represent the intensity with terms quadratic in the velocity. The representation of the line intensities are to this approximation:

$$\frac{I_b^-}{I_0} \;=\; 1 + \alpha_1 v_{\rm orb} + \alpha_2 v_{\rm orb}^2 \tag{32}$$

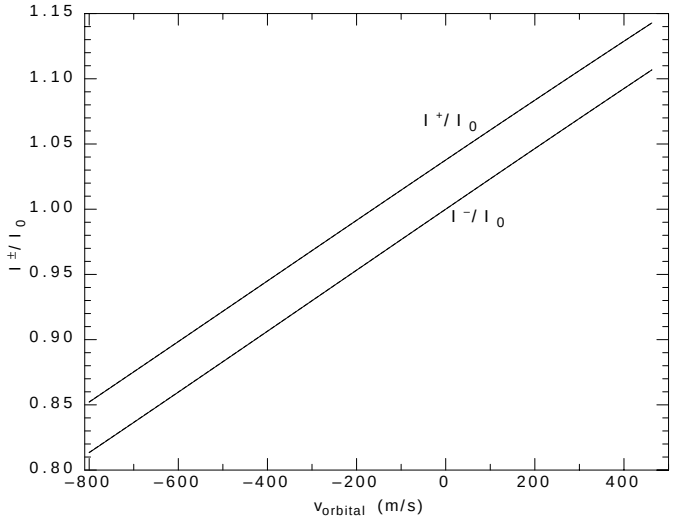

Fig. 8. The solar line intensity function $I_b^{\pm}/I_0$ as a function of the orbital velocity $v_{\rm orbital}$

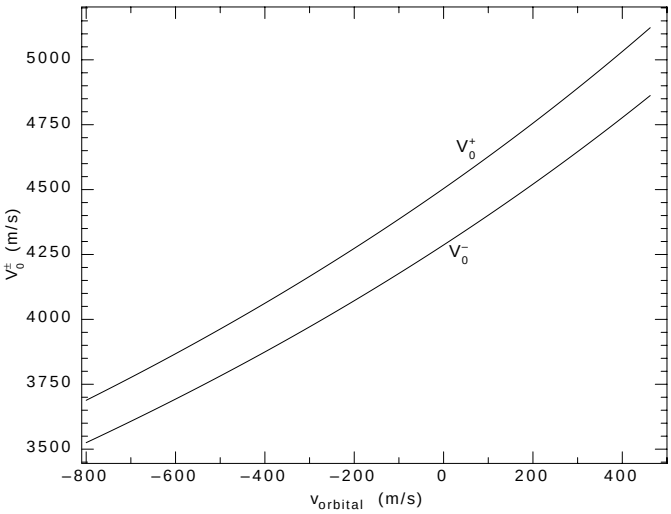

Fig. 9. The velocity sensitivity conversion factors $V_0^{\pm}$ as functions of the orbital velocity $v_{\rm orbital}$.

$$\frac{I_b^+}{I_0} = 1 + \alpha_1(v_{\rm orb} + \delta v) + \alpha_2(v_{\rm orb} + \delta v)^2 \quad (33)$$

$$= 1 + \alpha_1(1+\gamma_1)(v_{\rm orb} + v_e) + \\ +\alpha_2(1+\gamma_1)^2(v_{\rm orb} + v_e)^2 \,. \quad (34)$$

We can also represent I_b^+/I_0 as the product of I_b^-/I_0 and I_b^+/I_b^- from Eq. 31:

$$\frac{I_b^+}{I_0} = \frac{I_b^-}{I_0}\frac{I_b^+}{I_b^-} = \\ \left(1 + \alpha_1 v_{\rm orb} + \alpha_2 v_{\rm orb}^2\right)\left(1 + A_0 + A_1 v_{\rm orb}\right) . \quad (35)$$

We can equate these two expressions for I_b^+ and equate coefficients of like powers of $v_{\rm orb}$ to obtain two expressions for α_1 and α_2:

$$(1+\gamma_1)v_e\alpha_1 + (1+\gamma_1)^2 v_e^2\alpha_2 = A_0 \quad (36)$$

$$(\gamma_1 - A_0)\alpha_1 + 2(1+\gamma_1)^2 v_e\alpha_2 = A_1 \quad (37)$$

which are readily solved for α_1 and α_2. In the Appendix we show how to find the α_n for an arbitrary number of coefficients using as many empirically determined A_k as needed to represent the observed intensity ratio I_b^+/I_b^-. The signal functions S^+ and S^- are then

$$S_b^+ = \frac{I_0}{I_b^+}P_b^+ \quad \text{and} \quad S_b^- = \frac{I_0}{I_b^-}P_b^- \,. \quad (38)$$

The line intensity functions $I_b^{\pm}/I_0$ are shown in Fig. 8. The derivatives $(I_0)^{-1}dI_b^+/dv$ and $(I_0)^{-1}dI_b^-/dv$ can be calculated straightforwardly from these expansions allowing a V_0 function to be determined for S_b^+ and S_b^- individually. These sensitivity functions are shown in Fig. 9 as functions of the orbital velocity.

6. Velocities and detrending

The procedures described in the preceeding sections provide two functions $S^{\pm}$ and V_0 which are dependent on the sun-spacecraft line-of-sight velocity (note that the subscript indicating the application to the blue wing is dropped here since these applications will only be to the period between 11-Apr-1996 and 24-Jun-1998 for which the data was exclusively from the blue wing). The signal functions $S^{\pm}$ have been corrected for the line intensity variation and some instrumental effects but not for instrument aging and other possible instrument drifts. There are four separate signals to correct S_1^-, S_1^+, S_2^- and S_2^+ and these are treated independently. For the purpose of describing the process, the present discussion will be limited to only one of them: S_2^-. Results will be discussed for all channels in the following section. Because most of the effects treated by the detrending occur on long time scales, the figures presented here are for low pass filtered data sampled once per hour. The full reduced data set retains the 10 second sampling and is detrended for long time effects by the methods described here.

Fig. 10 shows S as a function of time. The nature of the variation is not understood, however, it appears to be the result of a decay modulated by some nearly sinusoidal process. Since we do not have any constraints we can place on the nearly sinusoidal process, we model this decay as the product of an exponential-like decay and a sinusoid with a phase function to be adjusted. To find the exponential-like decay, we need to examine periods when the nearly sinusoidal function has the same value. Lacking knowledge of times of equal phase for this function, we choose times when the uncertain phase will have the least impact, namely, those times when this function is at maxima or minima. Examination of Fig. 10 shows that there are two maxima and two minima. Imposing a requirement that the decay-corrected signal should be the same at the two maxima and the same at the two minima yields two conditions that allow us to adjust two constants in the decay formulation. Based on this plan we take the gain factor to be a quadratic exponential:

$$g(t) = \exp\left[\beta_1(t-t_0) + \beta_2(t-t_0)^2\right] \,. \quad (39)$$

Fig. 10 shows the product between S and this gain factor $g(t)$.

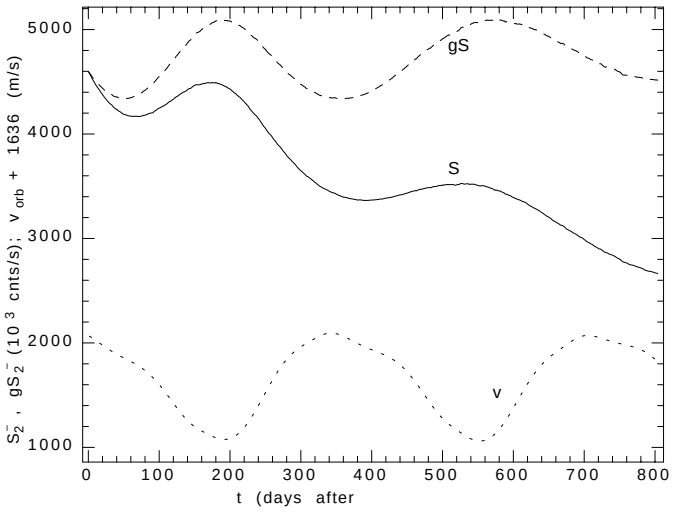

Fig. 10. The derived signal function S_2^- (solid) and the gain corrected function gS_2^- as a function of time (dashed). For comparison the orbital velocity is shown as well offset by $1\,\mathrm{km\,s^{-1}}$ plus the Einstein gravitational shift of $636\,\mathrm{m\,s^{-1}}$ (dotted).

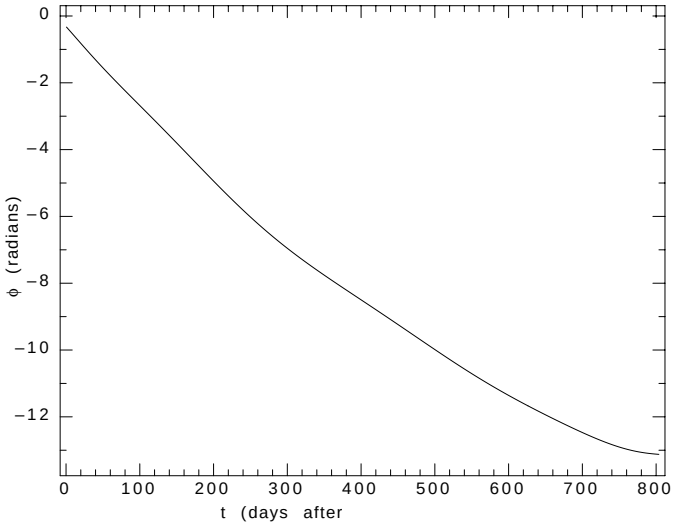

Fig. 11. The phase function $\phi(t)$ used to detrend the nearly sinusoidal drift of the intensity from the GOLF instrument. Shown is the phase function for photomultiplier 2 in the minus state of magnetic modulation.

Although the residual variation in gS is nearly sinusoidal and also nearly synchronous with the orbital velocity variations the initial and final turning points of gS do not coincide with the orbital velocity turning points and the orbital velocity is much further from a sinusoid than is gS. The cause for this variation is not understood but one can speculate that some interference effect perhaps a gradual change in the index of refraction of one cavity of the multi-layer band-pass filter is gradually changing to produce this sinusoid-like variation in the overall throughput. Regardless of the cause, the trends can be removed by taking advantage of the near sinusoidal behavior. To accomplish this a phase function $\phi(t)$ is derived so that a fitting function $z(t)$ of the form $z(t) = (gS)_0\,(1 + \epsilon \sin[\phi(t)])$ matches the time dependence of gS. The fit is carried out iteratively in the following sequence: 1) coefficients β_1 and β_2 in Eq. (39) are guessed and a trial value for gS is computed; 2) the turning points in gS are found by fitting a 4th order polynomial to gS in the vicinity of each turning point and then finding either maximum or minimum of this polynomial; 3) the two coefficients β_1 and β_2 are adjusted to cause the two maxima and two minima to have equal values of gS. Following step 3) the process can be repeated until the values of β_1 and β_2 are adequately stable. The interdependence between the fitting function z and gS depends on the proximity of the turning points: near the turning points z mostly depends on $(gS)_0$ and ϵ but is independent of ϕ while midway between the turning points z is most sensitive to ϕ.

The quantity $(gS)_0$ is the average of gS at the maximum and minimum turning points. While the fitting parameters β_1, β_2 and ϵ all must be determined numerically to high precision in order to leave a small remainder, the exact values are of little interest. To modest precision, all four time series are fitted by the values $\beta_1 = 6.95 \times 10^{-4}$ (days)$^{-1}$, $\beta_2 = -4.8 \times 10^{-8}$ (days)$^{-2}$, and $\epsilon = 0.080$. The phase function is found from $\phi(t) = \sin^{-1}\left[\epsilon^{-1}\left(gS/(gS)_0 - 1\right)\right]$. This quantity is smoothed by replacing the point by point values with a 10th order polynomial $\phi_f(t)$. The phase function for PM2 in the minus magnetic modulation state is shown in Fig. 11. The other phase functions are indistinguishable on the scale of this plot.

Following the end of the time period shown here, the observations have been interrupted by the SOHO loss of attitude control and communications. Just prior to the end of the sequence shown, it is evident in Fig. 11 that the pattern of evolution of ϕ has changed. Following the recovery of SOHO, the GOLF instrument is operating in the red wing and the new data can be treated with an appropriately applied version of the method described here. This new data shows that the change in the ϕ evolution is caused by a decrease in ϵ. In the new data the times of the turning points continues to follow the pattern shown in Fig. 10 with g being extended from Eq. (39) with approximately constant β_1 and β_2. Thus the evolution of the system throughput due to the effects discussed in this section is largely independent of the operation of the instrument which was off during the SOHO loss of control period. Consequently, it is unlikely that the throughput loss is due to aging of the photomultipliers or a degradation in the sodium cell optics. The change in ϵ means that the fitting function derived above cannot be used in the reduction of the new GOLF time series.

The above detrending procedure reduces the amplitude of temporal components having periods longer than about one tenth of the full time period or about 80 days. We can now calculate the velocity from Eq. (25) by taking S_0 to be

$$S_0(t) \;=\; g^{-1}(t)(gS)_0\,(1 + \epsilon \sin[\phi_f(t)]) \qquad (40)$$

and using V_0 calculated from the orbital velocity as shown in Fig. 9. The resulting quantity $v = V_0(S/S_0 - 1)$ has dimensions of a velocity and is a mixture of line shift and intensity effects from large scale convection and magnetic activity as well as possible instrumental drifts. The independent treatment of the

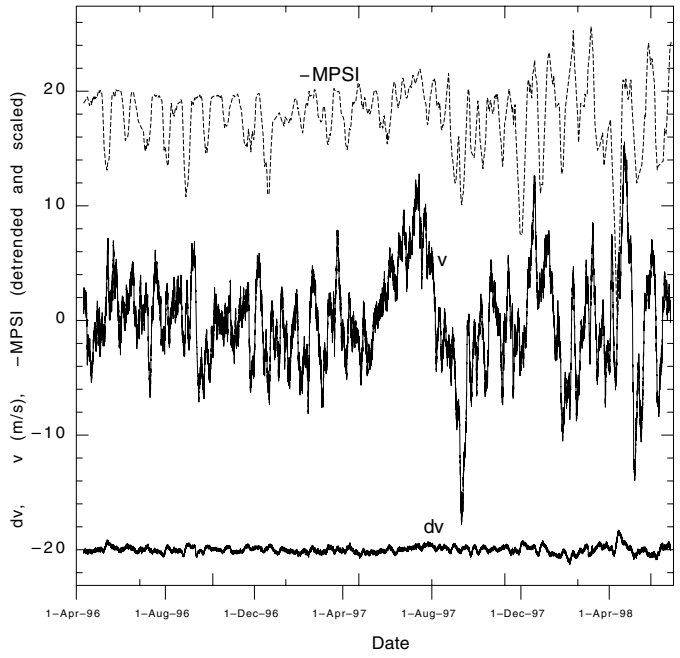

Fig. 12. This figure shows the velocity v and difference in velocity dv derived for PM2 according to the methods described in the text. The difference is the velocity from the plus state of magnetic modulation minus that for the minus state of magnetic modulation. The time series was subject to a low pass filter and then resampled to once per hour for this plot. The difference has been offset by -20 m s^{-1}.

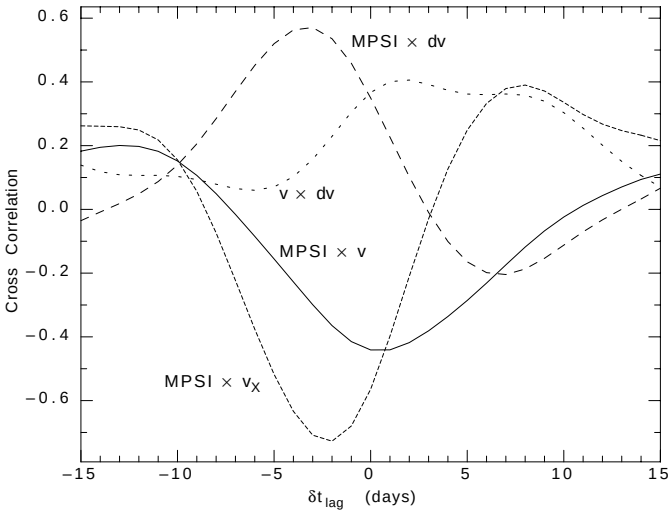

Fig. 13. The cross correlation functional dependency on the lag time δt. Each curve is labeled by the two functions which are included in the cross-correlation function. The lag δt is the amount by which the first function leads the second – i.e. where both functions change sign from positive to negative, a positive δt means the first function crosses zero before the second. The three velocity functions are explained in the text.

two states of magnetic modulation provides an indication of the differing effects of solar magnetic activity on the velocity derived from the intensity and the velocity derived from a local slope of the solar line. Fig. 12 shows the final velocity function, the difference in the velocity functions between the two states of magnetic modulation, and for reference a scaled and inverted plot of the MPSI(see the next paragraph). The difference function has been offset by -20 m s^{-1} in order to permit it to be seen easily. Each curve shows the result of a low pass filtered time series sampled once per hour. The above detrending procedure causes the overall trend lines to be of nearly zero slope. In the case of the difference velocity, it is of interest to point out that the temporal detrending is not required to bring the differences to near zero. The difference between the fitting functions relative to the fitting function itself is $(S_0^+ - S_0^-)/S_0 \approx \pm 2 \times 10^{-4}$ so that the line intensity determination is accurate to within one part per 500.

The long-time variation shown in Fig. 12 evidently has a periodicity close to the solar synodic rotation rate and is a consequence of the persistence of solar longitude zones of magnetic activity. In order to quantify this effect, we calculate the lagged cross-correlation coefficient between several velocity measures and an index of solar activity which has a high correlation with plage regions. This index, shown on Fig. 12, is called the Magnetic Plage Strength Index (MPSI) and has been developed by Chapman & Boyden (1986), Ulrich (1991) and Parker et al. (1998). Fig. 13 shows the cross-correlation function between the MPSI and the velocity v, the velocity difference $dv = v^+ - v^-$, and the velocity derived from the quantity $X = 0.5(P^+ + P^-)/\langle P^+ - P^- \rangle$ where the angle bracket notation implies a smoothing over one day. The velocities derived from X show the strongest correlation with solar activity but at a shifted lag time whereas the velocity derived directly from the intensity has the greatest correlation with no lag time. Evidently the darkening of the surface by sunspots and plages (for the GOLF working point of sodium) causes the effective velocity to be most negative when the spots and plages are nearest the center of the disk. For the quantities which depend on the line slope, dv and v_X the time of greatest cross-correlation is shifted from the time when these features are nearest disk center. Grec et al. (2000) have discussed a quantity σ which is similar to the inverse of X and found that it provides a means of studying the location of solar activity measured in a global fashion. A detailed comparison between the MPSI and specific excursions in the velocity derived from S shows that the features do line up as indicated by the cross-correlation but that the maximal excursions are a combination of uncorrected instrumental drift and the signal induced by the magnetic field features.

7. Results

We can utilize the velocity scaling and fitting to examine the solar background velocity variations and the dependence of the rms velocity amplitude on orbital velocity.

7.1. Power spectra

The power spectra for the velocity and the difference velocity are shown in Figs. 14 and 15 respectively. Also shown on the velocity power spectrum plot is a fit to the pattern based

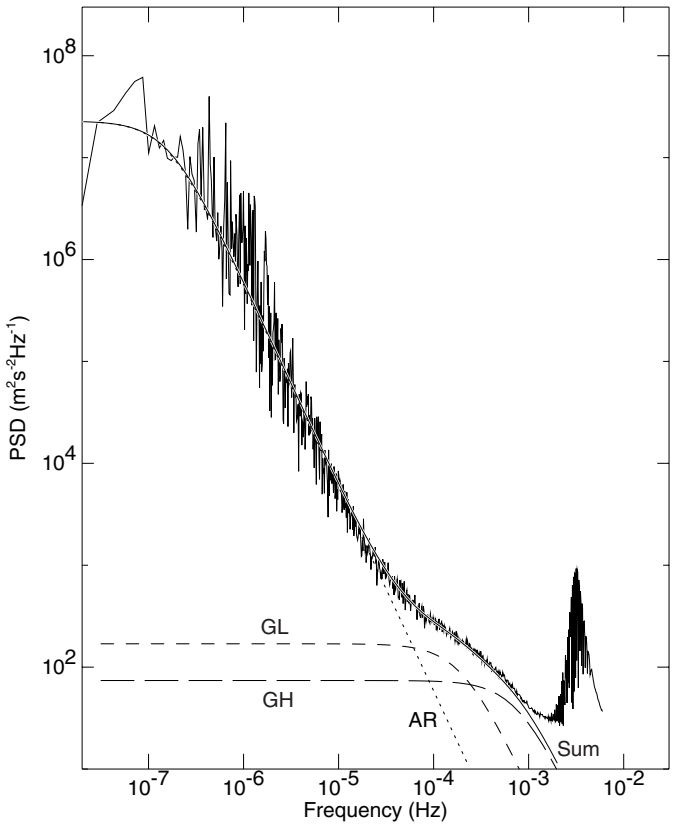

Fig. 14. This figure shows the log of the power spectrum versus the log of the frequency for the average of all four data channels (PM's 1 and 2 plus both states of magnetic modulation). The power spectral values have been binned into intervals of constant change in $\log(\nu)$.

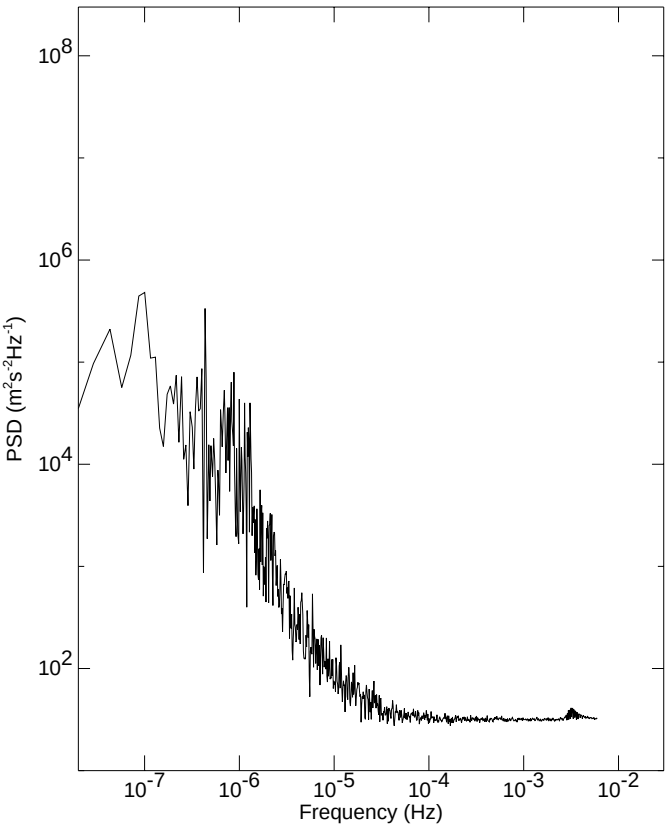

Fig. 15. This figure shows the log of the power spectrum of the difference in velocity between the plus and minus states of magnetic modulation versus the log of the frequency for the average of the data channels from PM 1 and 2. The power spectral values have been binned into intervals of constant change in $\log(\nu)$.

on the formula given by Harvey (1985) which uses only three components. This fit is discussed further in the next paragraph. An alternate treatment of the GOLF data (Robillot et al. 1998) calculates a velocity from a ratio which is related to quantities used in the present approach. The numerator of their ratio is proportional to the velocity derived here. The denominator of their ration at time scales longer than one day is proportional to our difference velocity while at time scales shorter than one day the denominator is essentially constant. One might expect there to be a break in the derived power spectrum related to the denominator smoothing if the numerator and denominator are correlated at time scales shorter than one day. Consequently, it is of interest to examine the components separately. The power spectrum from the velocity signal shown in Fig. 14 is based on an approach which deals with the GOLF data without any frequency dependent factors for all time periods between the 80 day limit from the phase function detrending and the cutoff of 6000 μHz imposed for convenience in this display which emphasizes the low frequency range. It provides an estimate of the solar background spectrum free from the effects of the diurnal cycles and atmospheric transparency problems of ground-based observers and takes advantage of the long and nearly continuous GOLF sequence. As such it represents an important estimation of the solar background spectrum. Previous power spectra including this wide range of frequencies have been published by Jiménez et al. (1988) and Pallé et al. (1995). At the lowest frequencies, the darkening effects of sunspots certainly can introduce a variability which is not a true velocity signal. Indeed, the considerations by Harvey (1985) anticipated that the velocity-like signal at periods comparable to the rotation period would be due to a cross-talk between intensity and velocity. We recognize this and simply refer to the time series as velocity signals even though some of what they include comes from intensity variations.

For the power spectrum derived from the velocity signal, there is a break in the slope at approximately 25 μHz. Below this frequency the slope matches that of the Harvey (1985) model for active regions with a slope of -2. The shape above the break is steeper than would be expected from the Harvey model for granulation alone although the break point is near where Pallé et al. (1995) showed the granulation and active region contributions crossing over. This change of slope suggests that the effects of active regions should become small in the frequency range of 100 to 1000 μHz where the search for low frequency solar modes is currently concentrated. Apparently the solar background in this frequency range is largely due to convective effects rather than magnetic and activity related effects. Between

about 50 μHz and 250 μHz the power spectral slope is about $-2/3$ while between 600 μHz and 1000 μHz the slope is steepest at -1.15. A change in slope of this type with a decrease toward lower frequency indicates a convective phenomenon with a lifetime comparable to the inverse of the frequency where the negative curvature in the power spectrum is greatest. This suggests the lifetime of the convective elements most responsible for the background noise is due to long-lived granulation. Based on these considerations, the fit to the Harvey formula utilizes only three components: an active region (AR) contribution with $a = 2.4\,\mathrm{m\,s^{-1}}$ and $\tau = 10^6$ s, a long-lived granulation (GL) contribution with $a = 0.23\,\mathrm{m\,s^{-1}}$ and $\tau = 800$ s, and a short-lived granulation (GH) contribution with an amplitude of $a = 0.3\,\mathrm{m\,s^{-1}}$ and $\tau = 205$ s. These two contributions represent parts of a distribution rather than distinct populations with well-defined properties. The amplitude and life-time parameters have the usual meaning of the Harvey power spectrum form where the power is $P = \sum_i a_i^2 \tau_i / \left(1 + (2\pi\nu\tau_i)^2\right)$. Due to the steepness of the low frequency part of the power spectrum, there can be no contribution from supergranulation or mesogranulation unless the contribution hypothesized for the active regions is steeper than the -2 slope adopted by the Harvey model.

We caution against a physical interpretation of the power spectrum shape in terms of the processes of granulation and supergranulation. The fact that a component having a range of lifetimes near that of the granulation should be present in the power spectrum while there can be no contribution from a component having the lifetime of supergranulation is very hard to explain on the basis of a physical model. If conservation of matter can cause the contribution from supergranulation to drop out, it should apply equally well to granulation and prevent the features with that lifetime from appearing in Fig. 14. It is probable that some other process must be invoked to explain the features seen in this power spectrum. Ulrich (1999) has suggested recently that atmospheric gravity waves have a resonance at the temporal frequency shown in Fig. 14 when driven by structures having a spatial wave number appropriate for supergranulation. This resonance response can alter the balance between the intensity and velocity components of the signal. The nature of the power spectrum shown in Fig. 14 clearly deserves additional attention.

The strongest peaks at the lowest frequencies correspond to 27 and 13 days and are the well-known rotational modulation associated with the active region signal (Jiménez 1988). The power spectrum of the difference velocity has a lower slope of $-5/3$ and is dominated by shot noise for frequencies above 11 μHz. When the difference signal is used to form a ratio prior to the calculation of a velocity, a low-pass filter is used to eliminate those frequency components above 11 μHz. Due to this shot noise, it is not possible to distinguish between convective and active region effects in the 100 to 1000 μHz frequency band in the case of the power spectrum of the difference velocity.

Distinct peaks or groups of peaks are found in the power spectrum of the velocity at periods of 26.9, 18.0, 9.0, 6.8 and 3.5 days. The peaks at 26.9, 18.0 and 3.5 days are distinct while those at 9.0 and 6.8 days are clusters. For the power spectrum of the difference in velocities, peaks at 27.0 and 9.0 days are clear while bands of enhanced power are seen near 13 and 7 days.

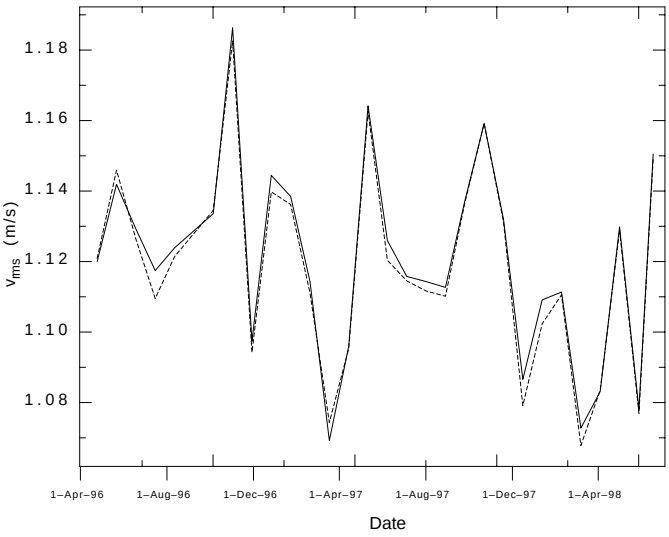

Fig. 16. This figure shows the rms velocity variability calculated from segments one synodic Carrington rotation in duration using a velocity time series filtered to remove components with periods longer than 4 hours. The solid and dotted lines are for the negative and positive magnetic modulation states respectively.

7.2. Amplitude in the 5-minute band

The velocity scaling derived in this paper depends on the determined line profile factors and even though the orbital velocity moves the GOLF working point on the solar line by $\pm$1nm, the scale factor included in V_0 should properly account for this variation. The scale factor V_0 changes by 30% during the year and differs between the two states of instrumental magnetic modulation by 4%. According to line contribution functions provided to us by Severino (1993), the height of formation using the Magain (1986) formulation varies between 242 and 310 km on the Vernazza et al. (1981) model C scale. These altitudes differ in density by 75% so that if the velocity scales as $\rho^{-1/2}$, the rms velocity should differ by 32% with the rms velocity being largest when the GOLF working point is closest to the line core at the most negative velocity. In addition, two states of magnetic modulation are offset from each other by an amount of 7% the orbital velocity range and should consequently show a difference in rms velocity of 2%.

In order to study the altitude dependence, the full time series was band-pass filtered to include only variations in the five-minute band having frequencies between 2000 μHz and 5000 μHz. The time sequence was divided into segments of 27.28 days, a period corresponding to one synodic Carrington rotation, and the rms variation in velocity was calculated for each. The results are shown in Fig. 16 for both states of magnetic modulation. One period including the time of the sodium cell cooldown in September of 1996 is left out because the gap

during the four days of no data has been filled with a noiseless auto-recursive representation which reduced the rms artificially for that Carrington rotation. It is clear from Fig. 16 that the observed dependence on altitude is much less than the estimate given here. By extracting the lowest four harmonic components from the time series of $v_{\rm rms}$ and comparing these components with the first four harmonic components from the orbital velocity, we find that variation in $v_{\rm rms}$ correlated with the change in the spectral line working point is only 3.3% instead of the anticipated 32%. In a similar fashion the average value of $v_{\rm rms}$ for the plus state of magnetic modulation is only 0.18 ± 0.05% smaller than that for the minus state instead of the expected 2%. Such a slight increase in the rms amplitude with altitude indicates that the modes are damped in this part of the sun's atmosphere.

8. Conclusions

This paper has developed a method for converting the signal from the GOLF instrument provided in its "one-wing" mode of operation into a quantity having dimensions of a velocity. An important time sequence is used from the "two-wing" period of operations to constrain the amplitude of the magnetic modulation. A formalism is presented to describe the three components of the scattered light and the interaction between their wavelengths and those of the solar absorption lines. The primary result of the method is to provide a sensitivity function V_0 which converts fractional photometric intensity deviations into a velocity. Such a method requires a reference intensity in order to calculate a deviation. We have presented a model of the GOLF signal which permits the retention of deviations having periods up to 45 days. The reference signal can also be obtained by temporally smoothing the photometric intensity and in this case the same sensitivity function continues to be appropriate.

Using the uniform treatment of the instrument for all time scales between 80 seconds and 80 days, we have provided an estimation of the shape of the sun's power spectrum. While uncertainties remain as to the relative importance of intensity and velocity contributions at low frequencies, the break in the power spectrum found at 25 μHz suggests that active region effects should be small in the frequency band between 100 and 1000 μHz. The very small variation found in the rms amplitude of the oscillatory signal as a function of sun-spacecraft shows that the kinetic energy density of the oscillation decreases with altitude. This is a consequence of the evanescent character of the acoustic oscillations in the photospheric layers combined with extra damping.

Acknowledgements. The development of GOLF over a period of several years owes a great deal to the skill and dedication of a large number of engineering and technical personnel at each of the participating institutes. The list of these colleagues has been given in the earlier instrument publication (Gabriel et al. 1995). We gratefully acknowledge the continued support (financial and otherwise) of the US National Aeronautics and Space Administration (NASA), the French Centre National d'Etudes Spatiales (CNES), the Commissariat à l'Energie Atomique (CEA) and the Spanish DGICYT under grant 95-0028-C.

Appendix A: derivation of the solar line intensity as a function of $v_{\rm orb}$

In order to convert the photomultiplier rate ratio to a function which represents the dependence of I_b on the orbital velocity we consider that I_b can be expanded in a power series of the orbital velocity and that I_b^+ and I_b^- are obtained by inserting $v^+ = v_{\rm orb} + \delta v$ and $v^- = v_{\rm orb}$ into this power series. According to Eq. (30) we can write:

$$v^+ = (1+\gamma_1)(v_{\rm orb} + v_e)\ . \tag{A.1}$$

The intensities can then be expressed in terms of the general power series:

$$I_b^- \ = \ I_0 \sum_{n=0}^{N} \alpha_n \, v_{\rm orb}^n \qquad \text{and}$$

$$I_b^+ \ = \ I_0 \sum_{n=0}^{N} \alpha_n (1+\gamma_1)^n (v_{\rm orb} + v_e)^n \tag{A.2}$$

where I_0 is the I_b^- intensity when $v_{\rm orb} = 0$ and for compactness of the sums we have defined $\alpha_0 = 1$. After utilizing the fact that $\gamma_1 v_{\rm orb} << 1$, the difference in intensities can be expressed as

$$\frac{I_b^+ - I_b^-}{I_0} \ = \ \sum_{n=0}^{N} \alpha_n \left[(1+n\gamma_1)(v_{\rm orb} + v_e)^n - v_{\rm orb}^n \right] \tag{A.3}$$

The quantity $(v_{\rm orb} + v_e)^n$ can be expanded as a binomial to get

$$\begin{aligned} (v_{\rm orb} + v_e)^n \ &= \ \sum_{m=0}^{n} \binom{n}{m} v_e^{n-m} v_{\rm orb}^m \\ &= \ \sum_{m=0}^{n-1} \binom{n}{m} v_e^{n-m} v_{\rm orb}^m + v_{\rm orb}^n \end{aligned} \tag{A.4}$$

After inserting the expansions for $(v_{\rm orb} + v_e)^n$ into Eq. (A.3) we get:

$$\begin{aligned} \frac{I_b^+ - I_b^-}{I_0} \ &= \ \sum_{n=0}^{N} \alpha_n (1+n\gamma_1) \\ &\quad \times \left[\sum_{m=0}^{n-1} \binom{n}{m} v_e^{n-m} v_{\rm orb}^m + v_{\rm orb}^n \right] \\ &\quad - \alpha_n v_{\rm orb}^n \end{aligned} \tag{A.5}$$

$$\begin{aligned} &= \ \sum_{n=0}^{N} \alpha_n \, (1+n\gamma_1) \sum_{m=0}^{n-1} \binom{n}{m} v_e^{n-m} v_{\rm orb}^m \\ &\quad + \sum_{n=0}^{N} \alpha_n n \gamma_1 v_{\rm orb}^n \end{aligned} \tag{A.6}$$

We seek to collect terms with like powers of $v_{\rm orb}$ and solve for the coefficients which result in Eq. (31) being satisfied for all values of $v_{\rm orb}$. In the double sum contained in Eq. (A.6) any particular power of $v_{\rm orb}$ can appear in more than one term. In order to collect all the terms having the same power of $v_{\rm orb}$

$$\begin{pmatrix} A_0 & -\binom{1}{0}(1+\gamma_1)v_e & -\binom{2}{0}(1+2\gamma_1)v_e^2 & \cdots & -\binom{n}{0}v_e^n \\ A_1 & (A_0-\gamma_1) & -\binom{2}{1}(1+2\gamma_1)v_e^2 & \cdots & -\binom{n}{1}v_e^n \\ A_2 & A_1 & A_0-2\gamma_1 & \cdots & -\binom{n}{2}v_e^n \\ \vdots & \vdots & \vdots & \ddots & \vdots \\ A_n & A_{n-1} & A_{n-2} & \cdots & A_0-n\gamma_1 \end{pmatrix} \times \begin{pmatrix} \alpha_0 \\ \alpha_1 \\ \alpha_2 \\ \vdots \\ \alpha_n \end{pmatrix} = 0 \qquad \text{(A.12)}$$

let us reverse the order of summation. We have to correctly set the limits of summation in the new order so that we continue to include the same terms originally present. As written in Eq. (A.6 the terms present have $0 \le n \le N$ and $0 \le m \le n-1$ so that when we exchange the order of the summation the limits transform as follows:

$$\sum_{n=0}^{N}\sum_{m=0}^{n-1} \longrightarrow \sum_{m=0}^{N}\sum_{n=m+1}^{N} \qquad \text{(A.7)}$$

which allows us to reexpress the intensity difference as:

$$\frac{I_b^+ - I_b^-}{I_0} = \sum_{m=0}^{N} a_m v_{\rm orb}^m \qquad \text{(A.8)}$$

where we have defined:

$$a_m = \alpha_m m\gamma_1 + \sum_{n=m+1}^{N} \alpha_n(1+n\gamma_1)\binom{n}{m} v_e^{n-m} \qquad \text{(A.9)}$$

We can combine Eqs. (31) and (A.8) for $(I_b^+ - I_b^-)/I_b^-$ and express the result as a function of $v_{\rm orb}$:

$$\frac{I_b^+ - I_b^-}{I_b^-} = \sum_{j=1}^{j_m} A_j v_{\rm orb}^j = \frac{\sum_{m=0}^{N} a_m v_{\rm orb}^m}{\sum_{n=0}^{N} \alpha_n v_{\rm orb}^n} \qquad \text{(A.10)}$$

The second half just comes from inserting the expansion for I^- into the denominator. This can be solved after multiplying by I_b^- on both sides to yield:

$$\left(\sum_{j=0}^{j_m} A_j v_{\rm orb}^j\right)\left(\sum_{n=0}^{N} \alpha_n v_{\rm orb}^n\right) = \sum_{m=0}^{N} a_m v_{\rm orb}^m \qquad \text{(A.11)}$$

After collecting the coefficients of like powers of $v_{\rm orb}^m$ we get the system of equations (see Eq. (A.12) on top of the page). This system can now be solved for all the α_n with $n > 0$ since $\alpha_0 = 1$ and all other quantities can be evaluated from the observations. Note that the A_i values need not differ from zero for more than A_0. In practice as indicated in Table 3 we have retained non-zero A_i for $i \le 2$. The equations also apply to the red wing data with the only change required being that of reversing the sign of δv_B. We could have retained the positive sign of δv_B and utilized a ratio P^-/P^+ but this would have involved a different weighting of the three scattering components. The method suggested here of retaining P^+/P^- and reversing the sign of δv_B leaves the three scattering components distributed nearly the same way relative to their average and provides a more symmetric treatment of the two wings. An IDL code to derive the α coefficients from the A coefficients is available from the UCLA GOLF website.

References

Boumier P. 1991, *PhD Thesis*, University of Paris VII.

Boumier P., Bocchia R., Damé L. et al. 1991, in B.H. Foing (ed.), *Proc. of the COSPAR ISCE Meeting ME.7 of the COSPAR Twenty-eighth Plenary Meeting, 'Helioseismology from Space'*, Pergamon Press, Oxford, p. 199.

Boumier P. & Damé L. 1993, Expimental Astron. 4, 87.

Boumier P., Decaudin M., Jones A.R., Grec G. and Tamiatto C. 1994, Experimental Astron. 4, 237.

Chapman G.A. and Boyden J.E. 1986, ApJ 302, L71.

Delbouille L., Roland G. and Neven L. 1973, *Photometric Atlas of the Solar Spectrum*, Inst. d' Astrophysique; Univ. Liège.

Dzitko H. 1995, *PhD Thesis*, University of Paris XI, Orsay.

Gabriel A.H., Grec G., Charra J., et al. 1995, Solar Phys. 162, 61.

Gabriel A.H., Charra J., Grec G., et al. 1997, Solar Phys. 175, 207.

García R.A. 1996, *PhD Thesis*, University of La Laguna, Tenerife, Spain.

García R.A., Roca Cortés T. and Régulo C. 1998, A&A Suppl. 128, 389.

García R.A., Turck-Chièze S., Robillot J.-M., et al. 2000, A&A in preparation.

García R.A., et al. 1997, *GOLF Annual Meeting*, Tenerife Spain.

Grec G., Renaud C., Boumier P. and García R.A. 2000, A&A in press.

Harvey J. 1985, in E. Rolfe & B. Battrick (ed.), *Future Missions in Solar, Heliospheric & Space Plasma Physics, esa sp-235*, ESA Publications, Noordwijk, p. 199.

Jiménez, A., et al. 1988, A&A 192, L7.

Magain P. 1986, A&A 163, 135.

Pallé P.L., et al.. 1995, ApJ 441, 952.

Pallé P.L., Régulo C., Roca Cortés T., et al. 1999, A&A 341, 625.

Parker D.G., Ulrich R.K. and Pap J.M. 1998, Solar Phys. 177, 229.

Reader J. and Corliss C.H. 1980, *Wavelengths and Transition Probabilities for Atoms and Atomic Ions - Part I. Wavelengths*, US-NBS: US Gov. Printing Office, Washington DC.

Renaud C., Grec G., Boumier P., et al. 1999, A&A 345, 1019.

Robillot J.-M., Turck-Chièze S., García R.A. et al. 1998, in S. Korzennik and A. Wilson (eds.), *Proc. SOHO 6/GONG 98 Workshop, 'Structure and Dynamics of the Interior of the Sun and Sun-like Stars'*, ESA Publications, Noordwijk, p. 317.

Severino G. 1993, private communication

Ulrich R.K. 1999, in SOI Team (ed.), *Proc. SOI Workshop: Helioseismology at Low Angular Degree, 9-11 December 1999, Stanford, CA*, SOI Team, Stanford, p. .

Ulrich R.K. 1991, in B.H. Foing (ed.), *Helioseismology from Space, COSPAR 28th Plenary Meeting, Adv. Space Res., vol. 11, no. 4*, Pergamon Press, p. Oxford;217.

Ulrich R.K., García R.A., Robillot J.-M., et al. 1998, in S. Korzennik and A. Wilson (eds.), *Proc. SOHO 6/GONG 98 Workshop, 'Structure and Dynamics of the Interior of the Sun and Sun-like Stars'*, ESA Publications, Noordwijk, p. 353.

Ulrich R.K., Boumier P., Robillot J.-M., García R.A., and Roca Cortés T. 2000, A&A in press.

Vernazza J.E., Avrett E.H. and Loeser R. 1981, ApJS 45, 635.